Lipid Rafts Alter the Stability and Activity of the Cholera Toxin A1 Subunit*�🅂

Supriyo Ray[‡], Michael Taylor[‡], Tuhina Banerjee[‡], Suren A. Tatulian[§], and Ken Teter[‡1]

From the [‡]Burnett School of Biomedical Sciences, College of Medicine, University of Central Florida, Orlando, Florida 32826 and the [§]Department of Physics, University of Central Florida, Orlando, Florida 32816

Background: Cholera toxin enters the target cell in a disordered state and must attain a folded, active conformation to modify its G protein target.
Results: Lipid rafts, where G protein is located, shift the disordered toxin to a functional conformation.
Conclusion: Lipids rafts provide a chaperone-like function for cholera toxin.
Significance: Lipid rafts play an important role in regulating toxin function through chaperone-like activity.

Cholera toxin (CT) travels from the cell surface to the endoplasmic reticulum (ER) as an AB holotoxin. ER-specific conditions then promote the dissociation of the catalytic CTA1 subunit from the rest of the toxin. CTA1 is held in a stable conformation by its assembly in the CT holotoxin, but the dissociated CTA1 subunit is an unstable protein that spontaneously assumes a disordered state at physiological temperature. This unfolding event triggers the ER-to-cytosol translocation of CTA1 through the quality control mechanism of ER-associated degradation. The translocated pool of CTA1 must regain a folded, active structure to modify its G protein target which is located in lipid rafts at the cytoplasmic face of the plasma membrane. Here, we report that lipid rafts place disordered CTA1 in a functional conformation. The hydrophobic C-terminal domain of CTA1 is essential for binding to the plasma membrane and lipid rafts. These interactions inhibit the temperature-induced unfolding of CTA1. Moreover, lipid rafts could promote a gain of structure in the disordered, 37 °C conformation of CTA1. This gain of structure corresponded to a gain of function: whereas CTA1 by itself exhibited minimal *in vitro* activity at 37 °C, exposure to lipid rafts resulted in substantial toxin activity at 37 °C. *In vivo*, the disruption of lipid rafts with filipin substantially reduced the activity of cytosolic CTA1. Lipid rafts thus exhibit a chaperone-like function that returns disordered CTA1 to an active state and is required for the optimal *in vivo* activity of CTA1.

Cholera toxin (CT)[2] exhibits an ADP-ribosyltransferase activity against the stimulatory α subunit of the heterotrimeric G protein ($G_s\alpha$) (1). ADP-ribosylation of Arg^{201} in $G_s\alpha$ locks the GTP-bound protein in an active state that promotes the continual stimulation of adenylate cyclase and its production of cAMP. Dysregulation of cAMP-dependent signaling pathways leads to the opening of apical chloride channels in intoxicated enterocytes. The osmotic movement of water to counterbalance chloride accumulation in the lumen of the gut consequently generates the profuse, life-threatening diarrhea of cholera.

CT has an AB_5 structural organization that consists of a catalytic A moiety and a homopentameric, cell-binding B moiety (2). For CT to manifest its latent ADP-ribosyltransferase activity, the CTA polypeptide must be proteolytically nicked to generate separate but disulfide-linked CTA1 and CTA2 subunits (3, 4). Nicking can involve *Vibrio* or other proteases. The disulfide bond linking CTA1 to CTA2 must then be reduced (4), which only occurs after the CT holotoxin moves from the cell surface to the endoplasmic reticulum (ER) through a series of vesicle-mediated trafficking steps collectively termed retrograde transport (5, 6). Reduction of the CTA1/CTA2 disulfide bond permits the chaperone-assisted dissociation of CTA1 from $CTA2/CTB_5$ (7, 8). CTA1 is held in a stable conformation by its interactions with the holotoxin (9, 10), but the isolated CTA1 polypeptide is an unstable protein that will spontaneously unfold at 37 °C upon its separation from $CTA2/CTB_5$ (11). The disordered CTA1 polypeptide is subsequently recognized as a misfolded protein by the host quality control system of ER-associated degradation (ERAD) (12–14). This results in the ER-to-cytosol translocation of CTA1 through one or more protein-conducting channels in the ER membrane (15–18). Most exported ERAD substrates are degraded by the ubiquitin-proteasome system, but the dearth of CTA1 lysine residues for ubiquitin conjugation allows the toxin to evade this fate (19, 20).

The translocated pool of CTA1 must regain a folded, active conformation to modify its $G_s\alpha$ target. This will not occur spontaneously because the isolated CTA1 polypeptide is in a disordered conformation at 37 °C (11). Host ADP-ribosylation factors (ARFs) act as allosteric activators of CTA1 and allow the toxin to exhibit *in vitro* catalytic activity at 37 °C (21, 22). However, it is possible that other host factors also assist the *in vivo* gain of structure and gain of function for cytosolic CTA1.

[1] To whom correspondence should be addressed: Biomolecular Research Annex, 12722 Research Pkwy., Orlando, FL 32826. Tel.: 407-882-2247; Fax: 407-384-2062; Email: kteter@mail.ucf.edu.

[2] The abbreviations used are: CT, cholera toxin; ARF, ADP-ribosylation factor; β_2AR, β_2-adrenergic receptor; DEA-BAG, diethylamino(benzylidineamino)guanidine; ER, endoplasmic reticulum; ERAD, ER-associated degradation; LUV, large unilamellar vesicle; PE, phosphatidylethanolamine; PS, phosphatidylserine.

A Chaperone-like Activity for Lipid Rafts

In this paper, we examined the impact of lipid rafts on the structure and function of CTA1. $G_s\alpha$ is found in lipid rafts at the cytosolic face of the plasma membrane (23–26). CTA1 would therefore encounter a lipid raft environment upon contact with its $G_s\alpha$ target. Because two major components of lipid rafts (cholesterol and phosphatidylethanolamine (PE)) can act as lipochaperones (27–29), we hypothesized an interaction with lipid rafts would shift disordered CTA1 to a folded, active conformation. Structural analysis with circular dichroism (CD) and functional analysis with an *in vitro* ADP-ribosylation assay supported our hypothesis: exposure to lipid rafts but not plasma membrane lipids allowed the disordered CTA1 subunit to attain a folded structure and enzymatic activity at 37 °C. The physiological relevance of these observations was documented with an *in vivo* intoxication assay which demonstrated intact lipid rafts are required for the ADP-ribosylation of $G_s\alpha$ by cytosolic CTA1. Lipid rafts thus display a chaperone-like activity that modulates the structure and function of CTA1.

EXPERIMENTAL PROCEDURES

Materials—The following were purchased from Avanti Polar Lipids (Alabaster, AL): cholesterol; palmitoyl sphingomyelin; 1-palmitoyl-2-oleoyl-*sn*-glycero-3-phosphocholine (POPC); 1,2-dioleoyl-*sn*-glycero-3-phospho-(1′-myoinositol) (DOPI); 1,2-dioleoyl-*sn*-glycero-3-phospho-(1′-myoinositol-4′-phosphate) (PI(4)P); 1,2-dioleoyl-*sn*-glycero-3-phospho-(1′-myoinositol-4′,5′-bisphosphate) (PI(4,5)P$_2$); 1-palmitoyl-2-linoleoyl-*sn*-glycero-3-phosphoethanolamine (PLPE); 1-palmitoyl-2-linoleoyl-*sn*-glycero-3-phospho-L-serine (PLPS); 1-stearoyl-2-arachidonoyl-*sn*-glycero-3-phosphocholine (SAPC); 1-stearoyl-2-arachidonoyl-*sn*-glycero-3-phosphoethanolamine (SAPE); 1-stearoyl-2-linoleoyl-*sn*-glycero-3-phosphoethanolamine (SLPE); 1-stearoyl-2-oleoyl-*sn*-glycero-3-phosphocholine (SOPC); and pyrene-labeled PE (pyrene-PE). Filipin was purchased from Santa Cruz Biotechnology (Santa Cruz, CA); CT was purchased from List Biologicals (Campbell, CA); and isoproterenol was purchased from Sigma-Aldrich. CTA1 with a C-terminal His$_6$ tag was purified as described previously (13) and used for all *in vitro* studies.

Composition and Generation of Large Unilamellar Vesicles (LUVs)—The plasma membrane lipid profile of the rat intestinal epithelium (30–34) was used as the basis for the acyl chain and head group composition of our plasma membrane mimic. Asymmetric lipid distributions between the inner and outer bilayer leaflets (35–37) were further considered to specifically model the composition of the inner leaflet of the plasma membrane (Table 1). To simulate the composition of a lipid raft (38–41), we mixed sphingomyelin and cholesterol with zwitterionic PE and anionic PS (Table 1). The latter two lipids are highly enriched in the inner leaflet of a lipid raft (42–45). Acyl chain selection was based upon the intestinal lipid composition. The inner leaflet of a lipid raft may lack sphingomyelin (46), so we formulated an alternative lipid raft mimic that lacked sphingomyelin (Table 1).

Individual lipids were dissolved in chloroform and mixed according to the percentages listed in Table 1. The total lipid concentration was 8 mM. The solvent was evaporated under a slow stream of nitrogen gas and vacuum dried for 4 h. The dried

TABLE 1

Lipid composition of LUVs mimicking the plasma membrane or lipid rafts

	Percentage of composition		
Lipid	Plasma membrane	Lipid raft	Variant lipid raft
Cholesterol	0	30	30
PLPS	13	15	15
Palmitoyl sphingomyelin	4	30	0
PLPE	27	25	45
SLPE	14	0	0
SAPE	5	0	0
SOPC	20	0	0
SAPC	14	0	0
PI(4,5)P$_2$	1	0	0
PI(4)P	1	0	0
DOPI	1	0	0
PLPC	0	0	10

mixture was suspended in 10 mM borate buffer (pH 7.0) containing 100 mM NaCl and vortexed thoroughly. To generate LUVs, the lipid mixture was passed 30 times through a Liposofast extruder (Avestin, Ottawa, ON, Canada) with 100-nm pore size polycarbonate membranes.

Membrane-binding Experiments—To detect CTA1 interaction with LUVs mimicking the composition of the plasma membrane or lipid rafts, we added 1% pyrene-PE to the vesicles. CTA1 was titrated with pyrene-PE-labeled vesicles in a 4 × 4-mm^2 path length quartz cuvette, and membrane binding of CTA1 was measured based on fluorescence resonance energy transfer (FRET) from the three tryptophan (Trp) residues of CTA1 to pyrene-PE using a Jasco 810 spectrofluoropolarimeter (Tokyo, Japan). This is a spectropolarimeter equipped with a Jasco PFD-425S Peltier temperature controller and an additional photomultiplier tube mounted at a right angle, which permits fluorescence measurements in addition to CD. Experiments were performed using a final sample volume of 220 μl containing 15 μM CTA1 in the presence or absence of LUVs, with excitation wavelength of 290 nm. The FRET data were analyzed as described previously (47). Briefly, changes in Trp fluorescence at each addition of pyrene-PE-containing vesicles (ΔF) were measured and plotted against $\Delta F/[L]$, where [L] is the total lipid concentration. These Scatchard plots were used to determine the limiting value of ΔF, *i.e.* ΔF_{max}. Protein binding isotherms were constructed by plotting $\Delta F/\Delta F_{max}$ against [L], after correction of ΔF values for the sample dilution effects and for the changes in ΔF in negative control experiments where the protein was titrated with vesicles without pyrene-PE. Using a Langmuir-type binding model (the membrane surface contains protein binding sites that bind the protein with a dissociation constant of K_D and a lipid-to-protein stoichiometry of N lipids/protein), values of K_D and N were determined from best fits of simulated and experimental binding isotherms.

CD and Fluorescence Spectroscopy—A Jasco 810 spectrofluoropolarimeter was used for CD measurements of samples placed in a 4-mm path length quartz cuvette. Experiments were performed using a final sample volume of 220 μl containing 15 μM CTA1 in the presence or absence of 800 μM LUVs. Light scattering effects became significant only below 205 nm in experiments with CTA1 and below 210–215 nm in experiments utilizing LUVs at 800 μM lipid concentration (*e.g.* see Fig. 2). The characteristic spectral minima of CD spectra which

were used for T_m determination (see below) were not affected by light scattering effects at this lipid concentration. To monitor the potential stabilizing effect of plasma membrane or lipid raft LUVs on CTA1 structure, near-simultaneous measurements of far-UV CD, near-UV CD, and fluorescence were taken as the temperature was increased stepwise from 20 °C to 60 °C. The temperature was ramped from 20 °C to 34 °C in 2 °C increments; from 34 °C to 40 °C in 1 °C increments, and from 40 °C to 60 °C in 2 °C increments. At each temperature, the sample was equilibrated for 4 min before measurement. The experimentally measured ellipticities (θ_{obs}) were converted to mean residue molar ellipticity, [θ], by using the following formula: [θ] = θ_{obs}/cnl, where n is the number of amino acid residues in the protein, c is the molar concentration of the protein, and l is the path length of the cuvette in millimeters.

Calculations of transition temperatures (T_m; the midpoint between folded and final disordered states) were performed as described previously (11). In brief, data were analyzed using the following equation (48):

$$X = f_L X_L + (1 - f_L) X_H \quad \text{(Eq. 1)}$$

where X is the measured temperature-dependent variable (*i.e.* the ellipticity or peak fluorescence emission wavelength), f_L is the fraction of amino acids representing the native conformation at low temperature, X_L is the limiting value of X at low temperature, and X_H is the limiting value of X at high temperature. The parameter, f_L, is given by:

$$f_L = \frac{\exp(-\Delta G/RT)}{1 + \exp(-\Delta G/RT)} \quad \text{(Eq. 2)}$$

The free energy of unfolding (ΔG) is given by

$$\Delta G = \Delta H(1 - T/T_m) + \Delta C\left[T - T_m - T\ln(T/T_m)\right] \quad \text{(Eq. 3)}$$

Here, ΔH is the apparent enthalpy of unfolding and ΔC (0.39 kcal mol^{-1} K^{-1}) is the heat capacity of unfolding.

To monitor the potential renaturation of disordered CTA1 by plasma membrane or lipid raft LUVs, far- and near-UV CD measurements of CTA1 structure were taken at 18 °C. Plasma membrane or lipid raft LUVs were added to a final lipid concentration of 800 μM after heating the toxin to 37 °C. The temperature was maintained at 37 °C, and CD spectra were recorded 5 or 30 min after exposure to the LUVs.

In parallel control experiments, CD and fluorescence measurements were recorded at each temperature in the presence of LUVs alone (plasma membrane, lipid raft, or variant lipid raft). CD and fluorescence spectra of the CTA1 samples were then corrected by subtraction of the appropriate temperature-matched spectra of LUVs only. Sphingomyelin produces a strong far-UV CD signal below 200 nm (*i.e.* between 195 and 197 nm), but around 220 nm its contribution to the far-UV CD signal is only 4–5% of the protein contribution (49). The minimal contribution of sphingomyelin to the 220 nm far-UV CD signal of CTA1 was eliminated by the aforementioned background subtraction procedure before calculating the CTA1 secondary structure T_m at 220 nm.

In Vitro Assay for CTA1 Catalytic Activity—Diethylamino-(benzylidine-amino)guanidine (DEA-BAG) is a CTA1 sub-strate that loses its ability to bind AG-50W-X4 ion exchange resin (Bio-Rad) after ADP-ribosylation (50). DEA-BAG also exhibits an intrinsic fluorescence (361-nm excitation wavelength, 440-nm emission wavelength), so the fluorescent signal remaining after pulldown with AG-50W-X4 resin represents the ADP-ribosylated pool of DEA-BAG. 2-fold serial dilutions of CTA1 were placed in 200 μl of KH$_2$PO$_4$ buffer (pH 7.5) containing 20 mM DTT, 10 mM NAD, and 0.1 mg/ml BSA. In a subset of samples, lipid raft LUVs were also added to a final lipid concentration of 800 μM. LUVs were added at 25 °C or after the toxin had been heated to 37 °C for 30 min. When added after heating, LUVs were incubated with the toxin for 1 h at 37 °C before addition of the DEA-BAG substrate. All toxin samples were incubated with 0.4 mg of DEA-BAG for 2 h at either 25 °C or 37 °C as indicated. After batch removal of unmodified DEA-BAG with 800 μl of a 40% AG-50W-X4 resin slurry, fluorescence intensity in the supernatant was recorded with a Biotek (Winooski, VT) Synergy 2 plate reader.

Cell Culture Studies—HeLa cells seeded to 80% confluence in 6-well plates were transfected with 0.5 μg of pcDNA3.1/mCTA1 (51) using a 5-h exposure to Lipofectamine (Invitrogen) according to the manufacturer's instructions. Transfected cells were chased in the absence or presence of filipin (1 μg/ml) for 2 or 4 h before cAMP levels were quantified using a commercial kit (PerkinElmer Life Sciences). Three samples per condition were run for each experiment. Background levels of cAMP from mock-transfected cells were subtracted from all results before expressing the data as percentages of the maximum cAMP signal obtained for the experiment.

CHO cells stably transfected with a gene encoding the β_2-adrenergic receptor (β_2AR) were provided by Dr. S. E. Mills (52, 53). Before quantification of cAMP levels, untreated and filipin-treated CHO-β_2AR cells were incubated for 4 h with 100 ng/ml CT or 1 μM β_2AR agonist isoproterenol. Filipin was co-incubated with CT or isoproterenol and was used at a concentration of 1 μg/ml. In each experiment, three samples were run for each condition. The basal levels of cAMP from untreated cells were subtracted from all results before expressing the data as percentages of the maximum cAMP signal obtained for the experiment.

RESULTS

CTA1 Binds to Lipid Rafts—Toxin-lipid interactions were initially examined by FRET (Fig. 1). CTA1 was incubated at 37 °C with LUVs mimicking the composition of either the plasma membrane or lipid rafts (Table 1). LUVs were prepared using 1% pyrene-PE at the expense of PLPE. Binding of CTA1 to the pyrene-PE-containing membrane results in short range dipolar interactions between the energy donor (Trp) and the acceptor (pyrene-PE), thus decreasing Trp emission intensity between 300 and 360 nm and increasing the 360–450 nm emission intensity of pyrene-PE. This FRET effect was observed when CTA1 was mixed with vesicles mimicking either the plasma membrane (Fig. 1*A*) or lipid rafts (Fig. 1*B*). As expected, increasing the LUV concentration produced a concomitant decrease in the Trp emission intensity. No substantial alteration to the CTA1 emission intensity was recorded when the toxin was incubated with plasma membrane (Fig. 1*C*) or lipid
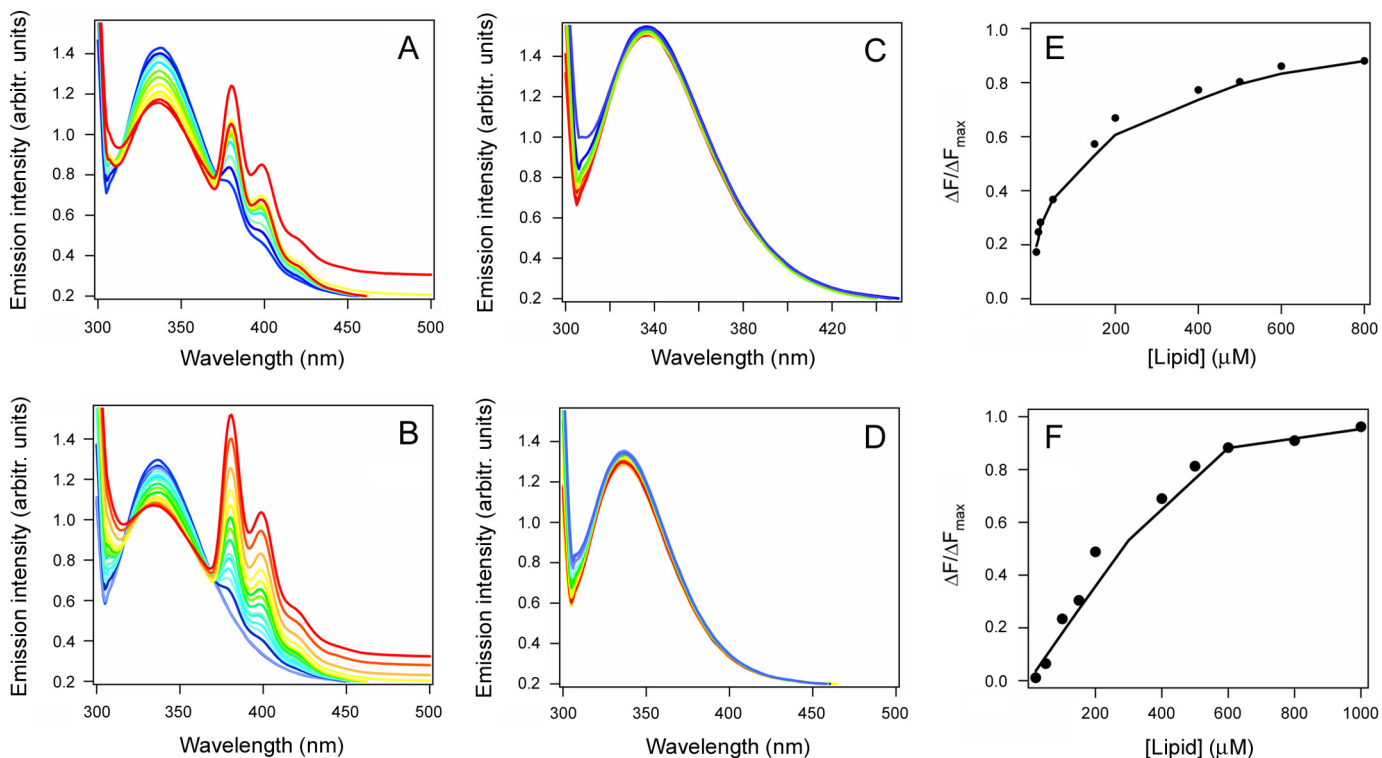
FIGURE 1. **CTA1 binds to plasma membrane and lipid raft LUVs.** The affinity between CTA1 and the plasma membrane (*A*, *C*, and *E*) or lipid rafts (*B*, *D*, and *F*) was determined by tryptophan FRET using pyrene-labeled LUVs (*A* and *B*) or unlabeled LUVs (*C* and *D*). For the representative spectra in *A–D*, a change of color from *blue* to *red* signifies an increase in lipid concentration from 100 to 1000 μM. Each measurement of fluorescent intensity for both labeled and unlabeled LUVs was normalized to the CTA1 concentration at the start of the experiment (*i.e.* corrections were made for the sample dilution effect). In *E* and *F*, the *solid lines* were constructed using a Langmuir-type binding model, and K_D values were calculated from curve fitting as described under "Experimental Procedures."

raft (Fig. 1*D*) LUVs lacking the pyrene-PE acceptor. The loss of CTA1 fluorescence intensity in Fig. 1, *A* and *B*, was therefore due to FRET between CTA1 and a membrane containing a pyrene-PE acceptor. Further data analysis was used to calculate a 2.3 μM K_D for CTA1 binding to plasma membrane LUVs (Fig. 1*E*) and a 0.6 μM K_D for CTA1 binding to lipid raft LUVs (Fig. 1*F*). CTA1 thus binds to both the plasma membrane and lipid rafts, but it has a higher affinity for lipid rafts.

The C-terminal A1$_3$ subdomain of CTA1 was initially thought to activate the ERAD system because this region contains a number of hydrophobic amino acid residues that could have allowed the toxin to masquerade as a misfolded protein (20). Subsequent studies found that the A1$_3$ subdomain is not essential for toxin translocation (54), but we hypothesized that this hydrophobic region is instead responsible for CTA1 binding to lipid bilayers. A CTA1 construct lacking the A1$_3$ subdomain (CTA1$_{1–168}$) was used to test this prediction. As shown in supplemental Fig. S1, CTA1$_{1–168}$ did not interact with either plasma membrane or lipid raft LUVs. CTA1$_{1–168}$ maintains the same stability and the same general structure as full-length CTA1 (12, 55), so the loss of binding affinity could not be attributed to structural alterations in CTA1$_{1–168}$. Thus, the hydrophobic A1$_3$ subdomain of CTA1 appeared to mediate toxin-lipid interactions directly.

Stabilization and Renaturation of CTA1 by Lipid Rafts—We next examined the structural impact of CTA1 binding to either the plasma membrane or lipid rafts. For this work, the thermal stability of CTA1 in the absence or presence of lipid bilayers was examined by CD and fluorescence spectroscopy (Fig. 2).

CTA1 was mixed with LUVs mimicking the composition of the plasma membrane or lipid rafts at 20 °C, and measurements were taken during a stepwise increase in temperature from 20 °C to 60 °C. Additional measurements were taken with a CTA1 sample heated in the absence of LUVs. The collective data demonstrated that interactions with plasma membrane and lipid raft LUVs have moderate and prominent stabilizing effects on CTA1, respectively. In the absence of LUVs, CTA1 exhibited a secondary structure transition temperature T_m of 34 °C (Fig. 2*A*), a tertiary structure T_m of 31 °C (Fig. 2*B*) derived from CD measurements, and a 34 °C T_m for the red shift to the maximum emission wavelength (λ_{max}) of Trp fluorescence (Fig. 2*C*). In the presence of plasma membrane LUVs, CTA1 exhibited a secondary structure T_m of 39 °C (Fig. 2*D*), a tertiary structure T_m of 37 °C (Fig. 2*E*), and a 37 °C T_m for the λ_{max} of Trp fluorescence (Fig. 2*F*). These values were similar to the corresponding T_m values recorded for CTA1 in the presence of LUVs mimicking the composition of the ER membrane (56), which suggests that toxin-lipid interactions may have a general stabilizing effect on the structure of CTA1. However, a substantially greater degree of stabilization was observed when CTA1 was exposed to lipid raft LUVs. For this condition, CTA1 exhibited a secondary structure T_m of 47 °C (Fig. 2*G*), a tertiary structure T_m of 45 °C (Fig. 2*H*), and a 44 °C T_m for the λ_{max} of Trp fluorescence (Fig. 2*I*). These T_m values were 10–14 °C higher than the values obtained for untreated CTA1 and 7–8 °C higher than the values recorded for CTA1 in the presence of plasma membrane LUVs, indicating a profound increase in CTA1 thermal stability upon interaction with membranes mimicking lipid
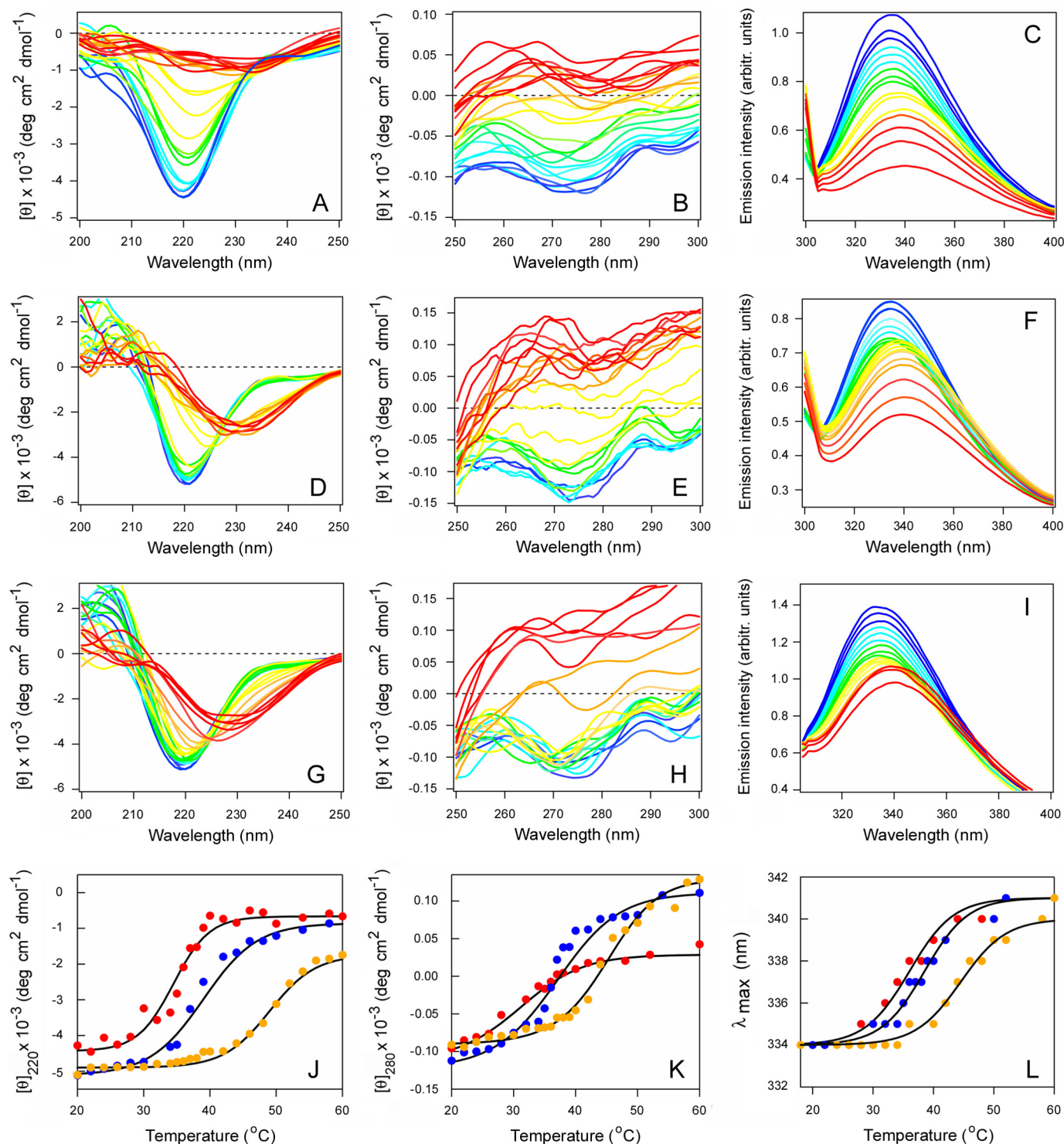
FIGURE 2. **CTA1 is stabilized by its interaction with plasma membrane and lipid raft LUVs.** The temperature-induced unfolding of CTA1 (*A–C*), CTA1 in the presence of plasma membrane LUVs (*D–F*), and CTA1 in the presence of lipid raft LUVs (*G–I*) was recorded by far-UV CD (*A, D,* and *G*), near-UV CD (*B, E,* and *H*), and fluorescence spectroscopy (*C, F,* and *I*). The change in color from *blue* to *red* denotes the increase in temperature from 20 °C to 60 °C. *J–L,* thermal unfolding profiles for CTA1 (*red*), CTA1 in the presence of plasma membrane LUVs (*blue*), and CTA1 in the presence of lipid raft LUVs (*orange*) were derived from the data presented in *A–I. J,* for far-UV CD analysis, the mean residue molar ellipticities at 220 nm ($[\theta]_{220}$) were plotted as a function of temperature. *K,* for near-UV CD analysis, the mean residue molar ellipticities at 280 nm ($[\theta]_{280}$) were plotted as a function of temperature. *L,* for fluorescence spectroscopy, the maximum emission wavelength (λ_{max}) was plotted as a function of temperature. One of two independent experiments is shown for each condition.

rafts. The thermal unfolding profiles for each of our biophysical measurements are shown in Fig. 2, *J–L,* and the calculated T_m values are summarized in Table 2. Neither plasma membrane nor lipid raft LUVs affected the thermal unfolding of

CTA1$_{1–168}$ (supplemental Fig. S2 and Table S1), which exhibits the same conformational stability as full-length CTA1 (12). Lipid-induced alterations to the structure of CTA1 thus required a direct interaction with the toxin.

CTA1 enters the cytosol in an unfolded state and must therefore regain an active, folded conformation to modify its $G_s\alpha$ target. We hypothesized that an interaction with lipid rafts would facilitate renaturation of the disordered CTA1 polypeptide. Far- and near-UV CD were used to test this prediction (Fig. 3). CTA1 was placed at 18 °C, and measurements of toxin structure were recorded. The toxin was subsequently heated to 37 °C. The disordered CTA1 polypeptide was then left untreated, was mixed with plasma membrane LUVs, or was mixed with lipid raft LUVs. Further measurements of toxin structure were recorded after an additional 5 min and 30 min at 37 °C. In the absence of LUVs, CTA1 progressed to an increasingly disordered state (Fig. 3, *A* and *B*). The presence of plasma membrane LUVs prevented the additional time-dependent loss of CTA1 structure but did not promote a gain of secondary or tertiary structure (Fig. 3, *C* and *D*). In contrast, CTA1 shifted to a more ordered state in the presence of lipid raft LUVs (Fig. 3, *E* and *F*). After 30 min at 37 °C in the presence of lipid rafts, the initially disordered CTA1 polypeptide displayed a microenvironment around its aromatic amino acid residues that was similar to the folded, 18 °C toxin conformation (Fig. 3*E*). The initial temperature-dependent loss of CTA1 secondary structure was also reversed in the presence of lipid rafts. However, the gain of CTA1 secondary structure was incomplete: the far-UV CD signal for raft-treated toxin was weaker than the initial 18 °C signal

TABLE 2
CTA1 stability in the presence of plasma membrane or lipid raft LUVs
Values represent the averages ± ranges from two independent experiments as represented by the data in Fig. 2 and supplemental Fig. S3.

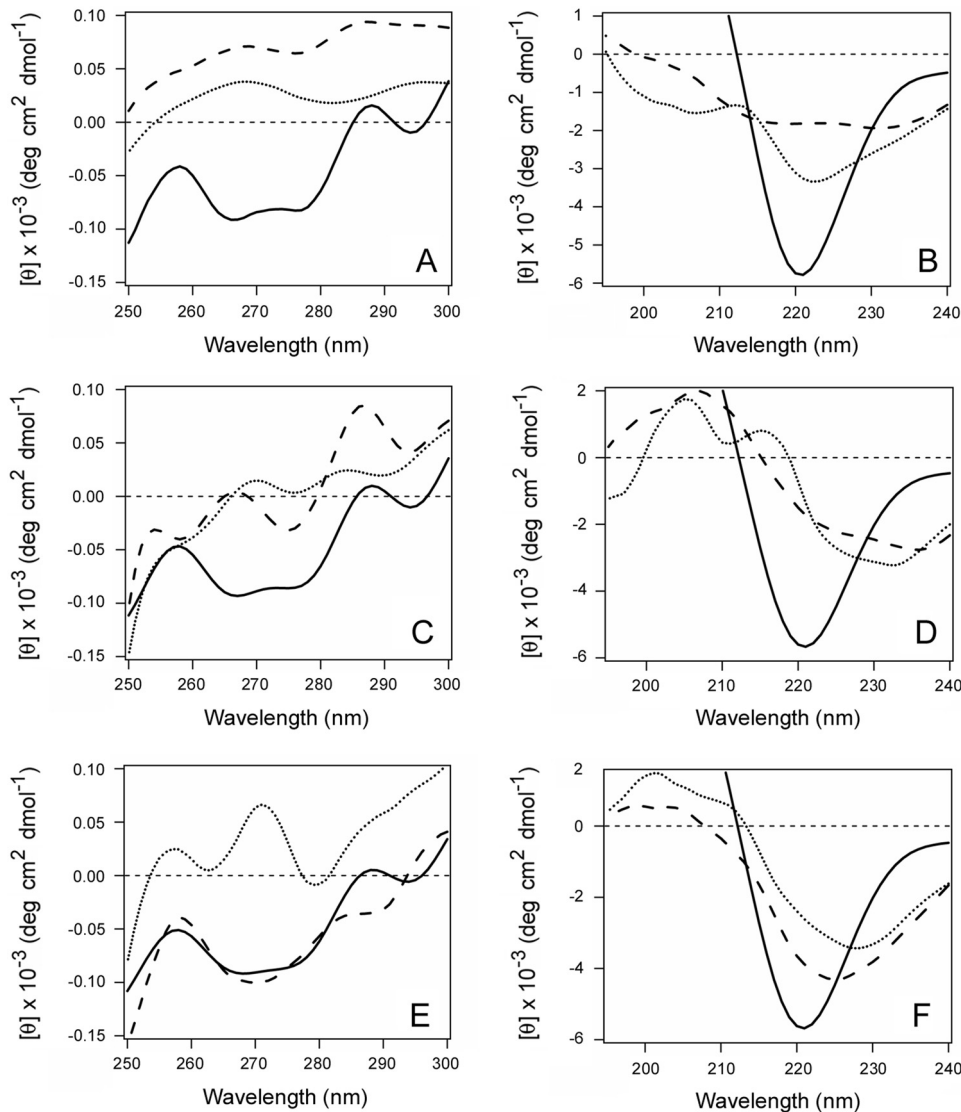| Toxin condition	T_m		
	Far-UV CD	Near-UV CD	Fluorescence spectroscopy
	°C	°C	°C
Untreated	34 ± 1	31 ± 1	34 ± 1
+Plasma membrane	39 ± 2	37 ± 1	37 ± 1
+Lipid raft	47 ± 2	45 ± 2	44 ± 1
+Variant lipid raft	45 ± 1	41 ± 1	41 ± 1

FIGURE 3. **Partial refolding of CTA1 by lipid raft LUVs.** CD was used to monitor the structure of CTA1. Measurements of untreated CTA1 were taken at 18 °C (*solid lines*). The toxin was subsequently heated to 37 °C and then left untreated (*A* and *B*), exposed to plasma membrane LUVs (*C* and *D*), or exposed to lipid raft LUVs (*E* and *F*). Additional near-UV CD (*A*, *C*, and *E*) and far-UV CD (*B*, *D*, and *F*) measurements were taken 5 (*dotted lines*) and 30 (*dashed lines*) min after a continued 37 °C incubation in the absence or presence of LUVs. One of three representative experiments is shown.

for folded CTA1 and was red-shifted by 4 nm from 220 to 224 nm, indicating the movement of amino acid residues into a more hydrophobic environment (Fig. 3*F*). A further 30-min incubation at 37 °C, for a total of 1 h in the presence of lipid raft LUVs, did not induce a further gain of structure in the CTA1 polypeptide (data not shown). These observations indicated that an interaction with lipid rafts at physiological temperature will promote a partial restoration of structure for the disordered CTA1 polypeptide.

Sphingomyelin may be largely restricted to the outer leaflet of a lipid raft (46), so we repeated our structural studies with variant lipid raft LUVs devoid of sphingomyelin (Table 1). The alternative, sphingomyelin-depleted lipid rafts also stabilized CTA1 when mixed with the toxin at 20 °C (supplemental Fig. S3) and induced a gain of CTA1 structure when mixed with the disordered toxin at 37 °C (supplemental Fig. S4). The stabilization of CTA1 by sphingomyelin-depleted lipid rafts was less prominent than that observed for sphingomyelin-containing lipid rafts but was still more substantial than the stabilization provided by plasma membrane lipids (Table 2). Moreover, sphingomyelin-depleted lipid rafts but not plasma membrane lipids could promote a gain of structure in disordered CTA1. These collective observations indicated that the presence of sphingomyelin is not critical for the dramatic structural alterations to CTA1 that result from its interaction with lipid rafts.

CTA1 Activity at Physiological Temperature Is Enhanced by Lipid Rafts—The isolated CTA1 polypeptide has little to no enzymatic activity at 37 °C (22), which is consistent with the disordered conformation it assumes at physiological temperature (11). We hypothesized the stabilization and renaturation of CTA1 by lipid rafts would allow the toxin to manifest its enzymatic function at 37 °C. This prediction was tested using DEA-BAG, a synthetic substrate for the ADP-ribosyltransferase activity of CTA1 (50). At 25 °C, we documented the dose-dependent modification of DEA-BAG by CTA1 (Fig. 4). A minimal signal was recorded at 37 °C, and this signal most likely represented a background reading because it did not increase with increasing toxin concentration. However, a substantial signal was detected when CTA1 was mixed with lipid raft LUVs before warming to 37 °C. The stabilizing effect of lipid rafts thus allowed CTA1 to maintain enough of its native structure, and hence activity, to effectively modify the DEA-BAG substrate. Moreover, CTA1 exhibited high levels of ADP-ribosylation activity when lipid raft LUVs were added after the toxin had been warmed to 37 °C. An interaction with lipid rafts thus shifted the disordered, 37 °C conformation of CTA1 to an active state. However, lipid rafts did not enhance the activity of folded CTA1 at 25 °C. The raft-induced gain of CTA1 function thus appeared to result from a gain of structure in disordered CTA1 rather than from allosteric activation of the toxin: if lipid rafts acted as an allosteric activator for CTA1, we would have also detected raft-stimulated toxin activity at 25 °C. These results were obtained with both sphingomyelin-containing lipid raft LUVs (Fig. 4) and sphingomyelin-depleted lipid raft LUVs (supplemental Fig. S5). Thus, sphingomyelin was not required for the raft-induced gain of CTA1 function at 37 °C.
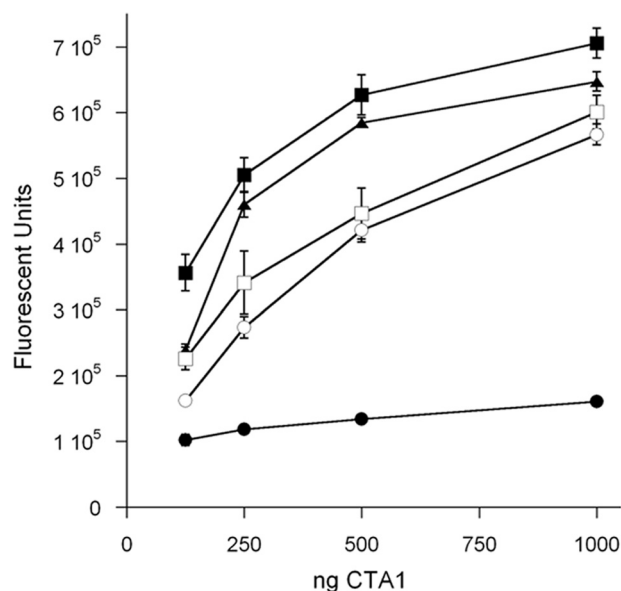

FIGURE 4. **CTA1 activity in the presence of lipid raft LUVs.** 2-fold dilutions of CTA1 were mixed with lipid raft LUVs at 25 °C for toxicity assays performed at 25 °C (*open squares*) or 37 °C (*filled squares*). For a third condition, LUVs were added after the toxin had been heated to 37 °C for 30 min (*filled triangles*). This toxin-LUV mixture was incubated at 37 °C for an additional hour before initiating the toxicity assay. Toxin samples incubated in the absence of LUVs at 25 °C (*open circles*) or 37 °C (*filled circles*) were also used for the assay. Four samples were used for each condition; results are presented as means ± S.E. (*error bars*). One of three representative experiments is shown.

In Vivo Contribution of Lipid Rafts to G Protein and CTA1 Function—$G_s\alpha$ is found in lipid rafts on the cytoplasmic face of the plasma membrane (23–26). CTA1 would thus encounter a lipid raft environment upon contact with its $G_s\alpha$ target. This suggests that lipid rafts could contribute to CT intoxication by facilitating the return of disordered CTA1 to a folded, active conformation. To examine this possibility, we monitored the enzymatic activity of CTA1 in filipin-treated cells. Filipin blocks CT intoxication by disrupting the lipid rafts which are required for endocytosis and intracellular trafficking of CT (57). To circumvent the upstream roles of lipid rafts in CT intoxication, we used a plasmid-based system (51) for direct expression of CTA1 in the cytosol of cells with intact or filipin-disrupted lipid rafts. At 2 and 4 h after transfection, filipin-treated cells exhibited substantially lower levels of cAMP than the untreated control cells (Fig. 5). Preliminary control experiments ensured that filipin did not alter the level of protein synthesis in drug-treated cells (data not shown), so the low levels of cAMP in filipin-treated cells could not be attributed to the lack of plasmid-borne CTA1 expression. Additional control experiments found that filipin treatment had a moderate, direct effect on $G_s\alpha$ signaling events: when treated with isoproterenol, a ligand for the G-coupled β_2AR (52, 53), CHO-β_2AR cells produced a robust cAMP response that was reduced by 20% in the presence of filipin. In contrast, filipin reduced the cAMP response from CTA1-expressing cells by 50% at 2 h after transfection and 65% at 4 h after transfection (Fig. 5). The greater extent of inhibition for CTA1-generated cAMP *versus* isoproterenol-generated cAMP indicated a direct inhibitory effect of filipin on the cytosolic activity of CTA1. Thus, lipid rafts appear to be essential for the optimal *in vivo* ADP-ribosyltransferase
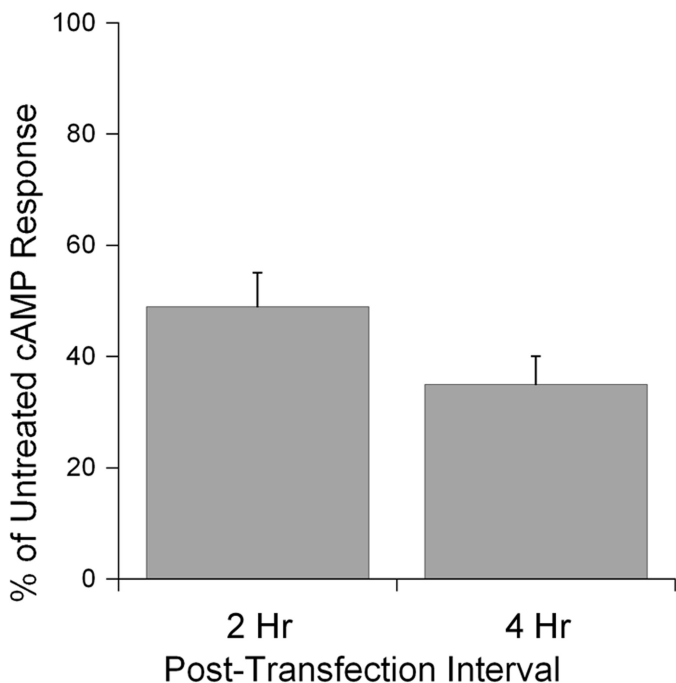
FIGURE 5. Lipid rafts are required for optimal *in vivo* activity of cytosolic CTA1. HeLa cells were transfected with a plasmid encoding a CTA1 construct that is expressed directly in the cytosol. Intracellular cAMP levels at 2 and 4 h after transfection were then quantified for untreated and filipin-treated cells. The averages ± S.D. (*error bars*) of 3–4 independent experiments with triplicate samples are shown.

activity of CTA1. Our *in vitro* biophysical and biochemical studies strongly suggest that the essential function of lipid rafts is linked to their chaperone-like ability to place disordered CTA1 in a folded, active conformation at 37 °C.

DISCUSSION

To reach its G protein target, CTA1 undergoes what has been termed an order-disorder-order transition (55). The ordered CTA1 polypeptide travels from the cell surface to the ER as part of an intact holotoxin (6). Separation of CTA1 from CTA2/CTB$_5$ in the ER releases the structural constraints on CTA1 unfolding and allows the dissociated CTA1 subunit to spontaneously assume a disordered conformation at physiological temperature (11). This unfolding event identifies CTA1 as a substrate for ERAD-mediated translocation to the cytosol (12–14, 58, 59). The translocated, cytosolic pool of CTA1 must then interact with one or more host factors to regain an ordered conformation. We have previously focused on the order-to-disorder transition that occurs in the ER. Here, we demonstrate lipid rafts play an active role in the disorder-to-order transition for cytosolic CTA1.

As documented with biophysical and biochemical assays, lipid rafts induced disordered CTA1 to assume an ordered, functional conformation. Lipid rafts thus exhibit a chaperone-like activity for CTA1. *In vivo* disruption of lipid rafts with filipin further demonstrated the physiological importance of this chaperone-like function, because the enzymatic activity of cytosolic CTA1 was greatly attenuated in filipin-treated cells. PE, a major component of the lipid raft inner membrane and the bacterial plasma membrane, is known to exhibit a "lipochaperone" function in the biogenesis of the polytopic bac-

terial protein lactose permease (29). Dimyristoylphosphatidylethanolamine can likewise induce denatured horseradish peroxidase to attain a folded, active conformation (27). In addition, cholesterol but not sphingolipid has been linked to the proper folding and maturation of cellular prion protein in the ER (28). Because multiple components of the lipid raft inner membrane can modulate protein structure, the chaperone-like activity observed for raft-CTA1 interactions could be a common phenomenon for raft-associated proteins.

Association of the CTB pentamer with its GM1 receptor results in toxin/ganglioside clustering in lipid rafts and subsequent internalization to the endosomal system. Continued interaction with the raft-associated GM1 then directs CT from the endosomes to the *trans*-Golgi network en route to the ER translocation site (6). Disruption of lipid rafts with filipin or methyl-β-cyclodextrin thus protects cultured cells from intoxication by inhibiting the endocytosis and intracellular transport of CT (57, 60). Given that CT delivery to the ER is dependent upon lipid rafts, the other important function of lipid rafts (*i.e.* modulation of cytosolic CTA1 structure/function) has gone undetected. We were able to document the *in vivo* chaperone-like function of lipid rafts toward CTA1 by directly producing CTA1 in the cytosol of cells transfected with the pcDNA3.1/mCTA1 expression vector. This bypassed the upstream raft-dependent CT trafficking events and allowed us to demonstrate an additional role for lipid rafts in the intoxication process. However, the cytosolic pool of transfected CTA1 still exhibited some activity in filipin-treated cells. This suggests that other components of the host cytosol, such as ARF proteins, could also contribute to the *in vivo* renaturation of disordered CTA1.

In previous work, filipin was applied to Caco-2 cells at various postintoxication time intervals (57). The inhibitory effect of filipin diminished with longer postexposure delays in drug treatment, which suggested that filipin only affected early steps in the intoxication process. However, this procedure could not determine how much CTA1 had already reach G$_s\alpha$ at the time of drug treatment. The use of a cAMP phosphodiesterase inhibitor would further stabilize any cAMP that had already been produced at the time of drug treatment. Our plasmid-based system provided an alternative method to disrupt lipid rafts before CTA1 appearance/expression in the cytosol. Data generated from this approach indicated that the optimal activity of cytosolic CTA1 requires intact lipid rafts, which was consistent with our *in vitro* biophysical and biochemical analysis of CTA1-raft interactions.

LUVs mimicking the composition of the ER (56) or plasma membrane provide a stabilizing environment for the labile structure of CTA1. However, lipid raft LUVs provide a substantially greater stabilizing environment than either ER or plasma membrane LUVs. Moreover, the gain of structure for disordered CTA1 is a raft-specific event. Because G$_s\alpha$ is present in lipid rafts (23–26), CTA1 would benefit from the chaperone-like function of lipid rafts upon contact with its G protein target. The resulting gain of structure confers a basal level of activity to CTA1 without acting through allostery because no gain of function was recorded for CTA1 treated with lipid rafts at 25 °C. Host ARF proteins instead act as allosteric activators of CTA1 by inducing a conformational change in CTA1 which

allows NAD (the donor molecule for the ADP-ribosylation reaction) to readily access the toxin active site (21, 61). Ongoing studies are examining the relative contributions of lipid rafts and ARF proteins to CTA1 activity.

CTA1 exhibited a 2.3 μM affinity for the plasma membrane and a stronger 0.6 μM affinity for lipid rafts. This differential affinity suggests a possible mechanism for CTA1 delivery to raft-localized $G_s\alpha$. The translocated pool of CTA1 appears to reach its $G_s\alpha$ target by diffusion through the cytosol (51). Binding to the plasma membrane would capture cytosolic CTA1 and place it in the general vicinity of $G_s\alpha$. The membrane-associated CTA1 subunit would then undergo lateral diffusion along the inner leaflet of the plasma membrane and eventually accumulate in the much smaller surface area of lipid rafts, as it has a higher affinity for lipid rafts than the bulk plasma membrane. A two-stage diffusion trap involving an initial binding to the bulk plasma membrane and a subsequent partitioning into lipid rafts would improve the probability of toxin-target interactions compared with a $G_s\alpha$ contact mechanism involving random toxin diffusion through the cytosol. Sequential interactions with the plasma membrane and lipid rafts would also serve to first stabilize and then refold the disordered, cytosolic CTA1 polypeptide.

The hydrophobic $A1_3$ subdomain at the C terminus of CTA1 is responsible for toxin binding to lipid bilayers. Thus, although it is not required for ERAD-mediated toxin translocation (54), the $A1_3$ subdomain still plays a functional role in host-toxin interactions. C-terminal domains from the catalytic subunits of Shiga toxin and ricin, two other ER-translocating toxins, also interact with lipid bilayers and play important roles in intoxication (62–65). For ricin A chain, the C terminus has been shown to mediate an interaction with the negatively charged phospholipids of the ER membrane which results in toxin unfolding (62, 63). This would place ricin A chain in a translocation-competent conformation for ERAD-mediated export to the cytosol. The available data suggest a similar mechanism for translocation of the Shiga toxin A1 subunit (64–66), although this model has yet to be directly addressed. An early model of ERAD-mediated toxin translocation noted that multiple ER-translocating toxins contain A chains with hydrophobic C termini and suggested that this could allow the toxin A chains to masquerade as ERAD substrates (20). It now appears that the C termini of toxin A chains, at least for CTA1, ricin A chain, and Shiga toxin A1 chain, play a common role in intoxication. However, rather than serving as a direct trigger for ERAD activation, the C termini seem to facilitate toxin-lipid interactions that promote either toxin unfolding in the ER or toxin refolding in the cytosol.

REFERENCES

1. De Haan, L., and Hirst, T. R. (2004) Cholera toxin: a paradigm for multifunctional engagement of cellular mechanisms (review). *Mol. Membr. Biol.* **21,** 77–92
2. Spangler, B. D. (1992) Structure and function of cholera toxin and the related *Escherichia coli* heat-labile enterotoxin. *Microbiol. Rev.* **56,** 622–647
3. Kassis, S., Hagmann, J., Fishman, P. H., Chang, P. P., and Moss, J. (1982) Mechanism of action of cholera toxin on intact cells: generation of A1 peptide and activation of adenylate cyclase. *J. Biol. Chem.* **257,** 12148–12152
4. Mekalanos, J. J., Collier, R. J., and Romig, W. R. (1979) Enzymic activity of cholera toxin. II. Relationships to proteolytic processing, disulfide bond reduction, and subunit composition. *J. Biol. Chem.* **254,** 5855–5861
5. Majoul, I., Ferrari, D., and Söling, H. D. (1997) Reduction of protein disulfide bonds in an oxidizing environment: the disulfide bridge of cholera toxin A-subunit is reduced in the endoplasmic reticulum. *FEBS Lett.* **401,** 104–108
6. Wernick, N. L., Chinnapen, D. J., Cho, J. A., and Lencer, W. I. (2010) Cholera toxin: an intracellular journey into the cytosol by way of the endoplasmic reticulum. *Toxins* **2,** 310–325
7. Taylor, M., Banerjee, T., Ray, S., Tatulian, S. A., and Teter, K. (2011) Protein disulfide isomerase displaces the cholera toxin A1 subunit from the holotoxin without unfolding the A1 subunit. *J. Biol. Chem.* **286,** 22090–22100
8. Tsai, B., Rodighiero, C., Lencer, W. I., and Rapoport, T. A. (2001) Protein disulfide isomerase acts as a redox-dependent chaperone to unfold cholera toxin. *Cell* **104,** 937–948
9. Goins, B., and Freire, E. (1988) Thermal stability and intersubunit interactions of cholera toxin in solution and in association with its cell-surface receptor ganglioside GM1. *Biochemistry* **27,** 2046–2052
10. Surewicz, W. K., Leddy, J. J., and Mantsch, H. H. (1990) Structure, stability, and receptor interaction of cholera toxin as studied by Fourier-transform infrared spectroscopy. *Biochemistry* **29,** 8106–8111
11. Pande, A. H., Scaglione, P., Taylor, M., Nemec, K. N., Tuthill, S., Moe, D., Holmes, R. K., Tatulian, S. A., and Teter, K. (2007) Conformational instability of the cholera toxin A1 polypeptide. *J. Mol. Biol.* **374,** 1114–1128
12. Banerjee, T., Pande, A., Jobling, M. G., Taylor, M., Massey, S., Holmes, R. K., Tatulian, S. A., and Teter, K. (2010) Contribution of subdomain structure to the thermal stability of the cholera toxin A1 subunit. *Biochemistry* **49,** 8839–8846
13. Massey, S., Banerjee, T., Pande, A. H., Taylor, M., Tatulian, S. A., and Teter, K. (2009) Stabilization of the tertiary structure of the cholera toxin A1 subunit inhibits toxin dislocation and cellular intoxication. *J. Mol. Biol.* **393,** 1083–1096
14. Taylor, M., Banerjee, T., Navarro-Garcia, F., Huerta, J., Massey, S., Burlingame, M., Pande, A. H., Tatulian, S. A., and Teter, K. (2011) A therapeutic chemical chaperone inhibits cholera intoxication and unfolding/translocation of the cholera toxin A1 subunit. *PLoS ONE* **6,** e18825
15. Schmitz, A., Herrgen, H., Winkeler, A., and Herzog, V. (2000) Cholera toxin is exported from microsomes by the Sec61p complex. *J. Cell Biol.* **148,** 1203–1212
16. Bernardi, K. M., Forster, M. L., Lencer, W. I., and Tsai, B. (2008) Derlin-1 facilitates the retro-translocation of cholera toxin. *Mol. Biol. Cell* **19,** 877–884
17. Saslowsky, D. E., Cho, J. A., Chinnapen, H., Massol, R. H., Chinnapen, D. J., Wagner, J. S., De Luca, H. E., Kam, W., Paw, B. H., and Lencer, W. I. (2010) Intoxication of zebrafish and mammalian cells by cholera toxin depends on the flotillin/reggie proteins but not Derlin-1 or -2. *J. Clin. Invest.* **120,** 4399–4409
18. Dixit, G., Mikoryak, C., Hayslett, T., Bhat, A., and Draper, R. K. (2008) Cholera toxin up-regulates endoplasmic reticulum proteins that correlate with sensitivity to the toxin. *Exp. Biol. Med.* **233,** 163–175
19. Rodighiero, C., Tsai, B., Rapoport, T. A., and Lencer, W. I. (2002) Role of ubiquitination in retro-translocation of cholera toxin and escape of cytosolic degradation. *EMBO Rep.* **3,** 1222–1227
20. Hazes, B., and Read, R. J. (1997) Accumulating evidence suggests that several AB-toxins subvert the endoplasmic reticulum-associated protein degradation pathway to enter target cells. *Biochemistry* **36,** 11051–11054
21. Welsh, C. F., Moss, J., and Vaughan, M. (1994) ADP-ribosylation factors: a family of approximately 20-kDa guanine nucleotide-binding proteins that activate cholera toxin. *Mol. Cell. Biochem.* **138,** 157–166
22. Murayama, T., Tsai, S. C., Adamik, R., Moss, J., and Vaughan, M. (1993) Effects of temperature on ADP-ribosylation factor stimulation of cholera

toxin activity. *Biochemistry* **32,** 561–566

23. Oh, P., and Schnitzer, J. E. (2001) Segregation of heterotrimeric G proteins in cell surface microdomains. G_q binds caveolin to concentrate in caveolae, whereas G_i and G_s target lipid rafts by default. *Mol. Biol. Cell* **12,** 685–698

24. Ostrom, R. S., and Insel, P. A. (2004) The evolving role of lipid rafts and caveolae in G protein-coupled receptor signaling: implications for molecular pharmacology. *Br. J. Pharmacol.* **143,** 235–245

25. Allen, J. A., Halverson-Tamboli, R. A., and Rasenick, M. M. (2007) Lipid raft microdomains and neurotransmitter signalling. *Nat. Rev. Neurosci.* **8,** 128–140

26. Kamata, K., Manno, S., Ozaki, M., and Takakuwa, Y. (2008) Functional evidence for presence of lipid rafts in erythrocyte membranes: $G_s\alpha$ in rafts is essential for signal transduction. *Am. J. Hematol.* **83,** 371–375

27. Debnath, D., Bhattacharya, S., and Chakrabarti, A. (2003) Phospholipid assisted folding of a denatured heme protein: effect of phosphatidylethanolamine. *Biochem. Biophys. Res. Commun.* **301,** 979–984

28. Sarnataro, D., Campana, V., Paladino, S., Stornaiuolo, M., Nitsch, L., and Zurzolo, C. (2004) PrP(C) association with lipid rafts in the early secretory pathway stabilizes its cellular conformation. *Mol. Biol. Cell* **15,** 4031–4042

29. Bogdanov, M., and Dowhan, W. (1999) Lipid-assisted protein folding. *J. Biol. Chem.* **274,** 36827–36830

30. Lencer, W. I., Chu, S. H., and Walker, W. A. (1987) Differential binding kinetics of cholera toxin to intestinal microvillus membrane during development. *Infect. Immun.* **55,** 3126–3130

31. Proulx, P. (1991) Structure-function relationships in intestinal brush-border membranes. *Biochim. Biophys. Acta* **1071,** 255–271

32. Forstner, G. G., Tanaka, K., and Isselbacher, K. J. (1968) Lipid composition of the isolated rat intestinal microvillus membrane. *Biochem. J.* **109,** 51–59

33. Waheed, A. A., Yasuzumi, F., and Gupta, P. D. (1998) Lipid and fatty acid composition of brush-border membrane of rat intestine during starvation. *Lipids* **33,** 1093–1097

34. Forstner, G. G., Sabesin, S. M., and Isselbacher, K. J. (1968) Rat intestinal microvillus membranes: purification and biochemical characterization. *Biochem. J.* **106,** 381–390

35. van Meer, G., Voelker, D. R., and Feigenson, G. W. (2008) Membrane lipids: where they are and how they behave. *Nat. Rev. Mol. Cell Biol.* **9,** 112–124

36. Boon, J. M., and Smith, B. D. (2002) Chemical control of phospholipid distribution across bilayer membranes. *Med. Res. Rev.* **22,** 251–281

37. D'Antuono, C., Fernández-Tomé, M. C., Sterin-Speziale, N., and Bernik, D. L. (2000) Lipid-protein interactions in rat renal subcellular membranes: a biophysical and biochemical study. *Arch. Biochem. Biophys.* **382,** 39–47

38. Dietrich, C., Bagatolli, L. A., Volovyk, Z. N., Thompson, N. L., Levi, M., Jacobson, K., and Gratton, E. (2001) Lipid rafts reconstituted in model membranes. *Biophys. J.* **80,** 1417–1428

39. Schroeder, F., Woodford, J. K., Kavecansky, J., Wood, W. G., and Joiner, C. (1995) Cholesterol domains in biological membranes. *Mol. Membr. Biol.* **12,** 113–119

40. Frazier, M. L., Wright, J. R., Pokorny, A., and Almeida, P. F. (2007) Investigation of domain formation in sphingomyelin/cholesterol/POPC mixtures by fluorescence resonance energy transfer and Monte Carlo simulations. *Biophys. J.* **92,** 2422–2433

41. Hammond, A. T., Heberle, F. A., Baumgart, T., Holowka, D., Baird, B., and Feigenson, G. W. (2005) Cross-linking a lipid raft component triggers liquid ordered-liquid disordered phase separation in model plasma membranes. *Proc. Natl. Acad. Sci. U.S.A.* **102,** 6320–6325

42. Pike, L. J., Han, X., Chung, K. N., and Gross, R. W. (2002) Lipid rafts are enriched in arachidonic acid and plasmenylethanolamine and their composition is independent of caveolin-1 expression: a quantitative electrospray ionization/mass spectrometric analysis. *Biochemistry* **41,** 2075–2088

43. Bakht, O., Pathak, P., and London, E. (2007) Effect of the structure of lipids favoring disordered domain formation on the stability of cholesterol-containing ordered domains (lipid rafts): identification of multiple raft-stabilization mechanisms. *Biophys. J.* **93,** 4307–4318

44. Delaunay, J. L., Breton, M., Trugnan, G., and Maurice, M. (2008) Differential solubilization of inner plasma membrane leaflet components by Lubrol WX and Triton X-100. *Biochim. Biophys. Acta* **1778,** 105–112

45. Grzybek, M., Kubiak, J., Łach, A., Przybyło, M., and Sikorski, A. F. (2009) A raft-associated species of phosphatidylethanolamine interacts with cholesterol comparably to sphingomyelin: a Langmuir-Blodgett monolayer study. *PLoS ONE* **4,** e5053

46. Brown, D. A., and London, E. (2000) Structure and function of sphingolipid- and cholesterol-rich membrane rafts. *J. Biol. Chem.* **275,** 17221–17224

47. Qin, S., Pande, A. H., Nemec, K. N., and Tatulian, S. A. (2004) The N-terminal α-helix of pancreatic phospholipase A2 determines productive-mode orientation of the enzyme at the membrane surface. *J. Mol. Biol.* **344,** 71–89

48. Lavigne, P., Crump, M. P., Gagné, S. M., Hodges, R. S., Kay, C. M., and Sykes, B. D. (1998) Insights into the mechanism of heterodimerization from the 1H-NMR solution structure of the c-Myc-Max heterodimeric leucine zipper. *J. Mol. Biol.* **281,** 165–181

49. Litman, B. J., and Barenholz, Y. (1975) The optical activity of D-erythro-sphingomyelin and its contribution to the circular dichroism of sphingomyelin-containing systems. *Biochim. Biophys. Acta* **394,** 166–172

50. Soman, G., Narayanan, J., Martin, B. L., and Graves, D. J. (1986) Use of substituted (benzylidineamino)guanidines in the study of guanidino group specific ADP-ribosyltransferase. *Biochemistry* **25,** 4113–4119

51. Teter, K., Jobling, M. G., and Holmes, R. K. (2004) Vesicular transport is not required for the cytoplasmic pool of cholera toxin to interact with the stimulatory α subunit of the heterotrimeric G protein. *Infect. Immun.* **72,** 6826–6835

52. Liang, W., Bidwell, C. A., Collodi, P. R., and Mills, S. E. (2000) Expression of the porcine β_2-adrenergic receptor in Chinese hamster ovary cells. *J. Anim. Sci.* **78,** 2329–2335

53. Mills, S. E., Kissel, J., Bidwell, C. A., and Smith, D. J. (2003) Stereoselectivity of porcine β-adrenergic receptors for ractopamine stereoisomers. *J. Anim. Sci.* **81,** 122–129

54. Teter, K., Jobling, M. G., Sentz, D., and Holmes, R. K. (2006) The cholera toxin A13 subdomain is essential for interaction with ADP-ribosylation factor 6 and full toxic activity but is not required for translocation from the endoplasmic reticulum to the cytosol. *Infect. Immun.* **74,** 2259–2267

55. Ampapathi, R. S., Creath, A. L., Lou, D. I., Craft, J. W., Jr., Blanke, S. R., and Legge, G. B. (2008) Order-disorder-order transitions mediate the activation of cholera toxin. *J. Mol. Biol.* **377,** 748–760

56. Ray, S., Taylor, M., Burlingame, M., Tatulian, S. A., and Teter, K. (2011) Modulation of toxin stability by 4-phenylbutyric acid and negatively charged phospholipids. *PLoS ONE* **6,** e23692

57. Orlandi, P. A., and Fishman, P. H. (1998) Filipin-dependent inhibition of cholera toxin: evidence for toxin internalization and activation through caveolae-like domains. *J. Cell Biol.* **141,** 905–915

58. Teter, K., and Holmes, R. K. (2002) Inhibition of endoplasmic reticulum-associated degradation in CHO cells resistant to cholera toxin, *Pseudomonas aeruginosa* exotoxin A, and ricin. *Infect. Immun.* **70,** 6172–6179

59. Teter, K., Jobling, M. G., and Holmes, R. K. (2003) A class of mutant CHO cells resistant to cholera toxin rapidly degrades the catalytic polypeptide of cholera toxin and exhibits increased endoplasmic reticulum-associated degradation. *Traffic* **4,** 232–242

60. Wolf, A. A., Fujinaga, Y., and Lencer, W. I. (2002) Uncoupling of the cholera toxin-G_{M1} ganglioside receptor complex from endocytosis, retrograde Golgi trafficking, and downstream signal transduction by depletion of membrane cholesterol. *J. Biol. Chem.* **277,** 16249–16256

61. O'Neal, C. J., Jobling, M. G., Holmes, R. K., and Hol, W. G. (2005) Structural basis for the activation of cholera toxin by human ARF6-GTP. *Science* **309,** 1093–1096

62. Day, P. J., Pinheiro, T. J., Roberts, L. M., and Lord, J. M. (2002) Binding of ricin A-chain to negatively charged phospholipid vesicles leads to protein structural changes and destabilizes the lipid bilayer. *Biochemistry* **41,** 2836–2843

63. Mayerhofer, P. U., Cook, J. P., Wahlman, J., Pinheiro, T. T., Moore, K. A., Lord, J. M., Johnson, A. E., and Roberts, L. M. (2009) Ricin A chain insertion into endoplasmic reticulum membranes is triggered by a temperature increase to 37 °C. *J. Biol. Chem.* **284,** 10232–10242

64. Menikh, A., Saleh, M. T., Gariépy, J., and Boggs, J. M. (1997) Orientation in lipid bilayers of a synthetic peptide representing the C terminus of the A1 domain of Shiga toxin: a polarized ATR-FTIR study. *Biochemistry* **36,** 15865–15872

65. Saleh, M. T., Ferguson, J., Boggs, J. M., and Gariépy, J. (1996) Insertion and orientation of a synthetic peptide representing the C terminus of the A1 domain of Shiga toxin into phospholipid membranes. *Biochemistry* **35,** 9325–9334

66. LaPointe, P., Wei, X., and Gariépy, J. (2005) A role for the protease-sensitive loop region of Shiga-like toxin 1 in the retrotranslocation of its A1 domain from the endoplasmic reticulum lumen. *J. Biol. Chem.* **280,** 23310–23318